

## Optimization and Process Modelling Of the Extraction of Iron Oxide from Aku Clay by Hydrochloric Acid Leaching

Onoh Ikechukwu Maxwell<sup>1</sup>, Mbah Gordian Onyebuchukwu<sup>2</sup>, Mbah-Iroulo Ebere Rita<sup>3</sup>

1, 2 & 3 Chemical Engineering Department, Enugu State University of Science and Technology (ESUT), P.M.B. 01660 Enugu, Nigeria.

\*Corresponding Author: Onoh Ikechukwu Maxwell

**ABSTRACT:** The study of extraction of iron oxide from 'Aku' clay by hydrochloric acid leaching was carried out. The clay was analyzed using Atomic Absorption Spectrophotometer (AAS) to determine the metallic ions present in the clay. SEM image of the residual clay showed some cracks after acid treatments which is an indication of effective leaching. Effect of process parameters such as calcination temperature, Leaching temperature, acid concentration, liquid-to-solid ratio, and contact time at constant speed of 500 rpm and particle size of 100  $\mu\text{m}$  were investigated. The Iron oxide leaching was optimized using central composite design of response surface methodology. The results obtained showed that the 'Aku' clay contained an appreciable percentage of iron oxide. It was observed that the yields of iron oxide increased as calcination temperature, leaching temperature, acid concentration, liquid-to-solid ratio, and contact time increased. The optimal conditions obtained for the leaching of iron oxide from the calcined Aku clay are 822°C calcination temperature, 67°C leaching temperature, acid concentration of 2.2M, liquid to solid weight ratio of 12.9 ml acid/1gm clay, and contact time of 61 minutes with a yield of 68.9%. The X-ray fluorescence spectrometer analysis showed 54.103 wt% Iron oxide extract. This study has shown that Aku clay can serve as an alternative raw material for the iron industries in Nigeria.

**KEYWORDS:** Acid leaching, Aku clay, Fourier transform infrared (FTIR), Iron oxide, Optimization,

Date of Submission: 25-05-2018

Date of acceptance: 09-06-2018

### I INTRODUCTION

Iron in form of oxide is a major component of clay. The characterization of several clays by different researchers revealed that most Nigerian clays are rich in iron oxide (Ogbemudia et al., 2010; Ajemba and Onukwuli, 2012; Ogbuagu et al., 2007; Lori et al., 2007). Iron oxides exist in a rich variety of structures and occur in a great variety of settings, from geological to nanoscale technological applications. Ferrous and ferric iron oxides present seven crystalline phases, the more common are  $\alpha\text{-Fe}_2\text{O}_3$  (hematite),  $\gamma\text{-Fe}_2\text{O}_3$  (maghemite),  $\text{Fe}_3\text{O}_4$  (magnetite) and  $\text{Fe}_{1-x}\text{O}$  (wustite); the less commonly found are the  $\beta\text{-}$  and  $\epsilon\text{-Fe}_2\text{O}_3$  phases and the low-temperature rhombohedral structure of magnetite (Arturo *et al.*, 2009). Iron (III) oxide or ferric oxide is the inorganic compound with the formula  $\text{Fe}_2\text{O}_3$ . It is one of the three main oxides of iron, the other two being iron(II) oxide (FeO), which is rare, and iron (II,III) oxide ( $\text{Fe}_3\text{O}_4$ ), which also occurs naturally as the mineral magnetite.  $\text{Fe}_2\text{O}_3$  is ferromagnetic, dark red, and readily attacked by acids. Iron (III) oxide is often called rust, and to some extent this label is useful, because rust shares several properties and has a similar composition. To a chemist, rust is considered an ill-defined material, described as *hydrated ferric oxide* (Housecroft & Sharpe, 2008). The overwhelming application of iron (III) oxide is as the feedstock of the steel and iron industries. It is used to put the final polish on metallic jewelry and lenses, and historically as a cosmetic (Sultana et al., 2014).

Leaching is a liquid-solid operation. The two phases are in intimate contact, the solute(s) can diffuse from the solid to the liquid phase, which causes a separation of the components originally in the solid. A special leaching process, when an undesirable component is removed from a solid with water, is called washing (Alafara et al., 2005). Generally there are five rate steps in the leaching process (Coulson & Richardson, 1991). Leaching is used to remove the metals from their ores, which contains many undesirable constituents, as solute

salts. Most dissolution studies of iron oxides have been confined to their preferential dissolution from soils so that other minerals could be concentrated and studied (Mitchell et al., 1964). Ambikadevi and Lalithambika (2000) in their investigation of several organic acids leaching of iron from clay found that oxalic acid is more efficient. The extent of the dissolution reaction depends on both clay mineral type and reaction conditions, such as the acid/clay ratio, acid concentration, time, and temperature of the reaction (Abali et al, 2006; Lui et al, 2010). Many researchers like Ozdemir and Cetisli, (2005), Ajemba and Onukwuli, (2012), Poppleton and Sawyer, (1977), Eisele, (1983), Al-Zahrani and Abdul, (2009) have identified calcinations temperature, leaching temperature, acid concentration, liquid-solid ratio and stirring speed to be very important process parameters that affects the leaching of minerals from clays.

However, this study was aimed at the optimization and evaluation of statistical modeling of the removal (leaching) of iron oxide from local clay (Aku clay) by the application of hydrochloric acid as the leachant.

## II MATERIALS AND METHOD

### 2.1 Sourcing of Raw materials

The raw clay was collected from 'Aku' in Enugu State Eastern Province of Nigeria with a Global Positioning System (GPS) Device, (Model; Etrex Germin), with Latitude; N05° 38.216<sup>1</sup>, Longitude; E07° 19.664<sup>1</sup>, and elevation above sea level; 623ft. The other materials used in the experimental work which included; distilled water, sodium hydroxide and hydrochloric acid was purchased from Ogbete main market Enugu, Nigeria.

### 2.2 Clay Preparation and Leaching Process

The clay was ground with a laboratory mortar and pestle and sieved to a particle size of 100µm. The Clay was calcined at temperatures between 600 C and 900 C. The calcined clay and the raw clay both at 100 µm particle size and 50 C leaching temperature underwent leaching process by mixing each sample with 3M Hydrochloric acid and 8cm<sup>3</sup>acid/1gm clay liquid to solid weight ratio. The mixture was then stirred at a constant speed of 500 rpm for 60 minutes contact time. After each leaching process, the leached liquor was collected and filtered using Whatman filter paper. 5ml of the filtrate was then withdrawn and analyzed using X-ray Fluorescence (XRF) to determine the amount of iron oxide present. The experiment was repeated to study the effect of process parameters.

### 2.3 Extraction of iron oxide

Iron oxide was extracted according to the method of Rasmita and Mamata (2011). The filtrate was introduced into a 250 ml conical flask. The pH meter was calibrated using buffer solutions of the following pH; 4, 6.8 and 9.80 as supplied by the manufacturer. The initial pH of the solution was found to be acidic. 1N sodium hydroxide solution was added to the leachate in drops until the pH was brought to 10. As the pH of the medium increased, reddish brown precipitates of iron (III) hydroxide were crystallized. The solution was filtered and the crystals collected in filter paper. The crystals (iron (III) hydroxide) were washed with 50ml of distilled water and dried in laboratory hot air oven. The whole dried residue was transferred to a porcelain crucible and ashed in a muffle furnace at 600°C for 4 hours. The iron (III) hydroxide was then converted to iron (III) oxide.

$$\% \text{ Iron oxide} = \frac{\text{wt of iron oxide crystallized out}}{\text{theoretical weight of iron oxide present in the raw / calcined clay}} \times 100 \quad (1)$$

### 2.4 Characterization of the raw and calcine clays

The physical properties of the raw and calcined clay were carried out using ASTM D7263-09(2017) methods. Instrumental of the samples was done using X-Ray Fluorescence (XRF) which is controlled by a PC running the dedicated Mini-Pal analytical software. The Mini-Pal 4 version used was PW 4030 X-ray Spectrometer running with voltage (30KV maximum) and a current (1mA maximum) to determine the mineral composition of the clay. Fourier transform infrared spectrometer was used to determine the chemical bond and functional groups in the clay samples. Consequently, Scanning Electron Microscopy (SEM) was used to determine the size and morphology of the clay samples. The SEM micro graph was obtained using JOEL scanning electron microscope model JSM 6400 Scanning electron microscopy recording at 15 KV with 8000x magnification.

### 2.5 Optimization of leaching process

The optimization of the leaching process was done using Central Composite Design of Response Surface Methodology. Design Expert software (version 9 trial version) was used in this study to design the experiment and to optimize the leaching yield. The experimental design employed in this work was a two-level-five factor fractional factorial design, involving 32 experiments. Calcination temperature, T<sub>c</sub>, Leaching temperature, T<sub>L</sub>, acid concentration, A, liquid-solid ratio, LS and contact time, CT were selected as independent factors for the optimization study. The response chosen was the metal yield obtained from leaching of the

calcined clay sample. Six replications of centre points were used in order to predict a good estimation of errors and experiments were performed in a randomized order. The actual and coded levels of each factor are shown in Table 2.1. The coded values are designated by  $-1$  (minimum),  $0$  (centre),  $+1$  (maximum),  $-\alpha$  and  $+\alpha$

**Table 2.1: Studied range of each factor in actual and coded form.**

Independent variables	Symbols	Range and levels				
		$-\alpha$	$-1$	$0$	$+1$	$+\alpha$
Calcinations temp. ( $^{\circ}\text{C}$ )	A	600	700	800	900	1000
Leaching temp. ( $^{\circ}\text{C}$ )	B	30	50	70	90	110
Acid conc. ( $\text{mol}/\text{dm}^3$ )	C	0.75	1.5	2.25	3.0	3.75
Liquid-solid ratio ( $\text{cm}^3/\text{g}$ )	D	4	8	12	16	20
Contact time (min)	E	20	40	60	80	100

**Table 2.2: Experimental Design Matrix for Metallic Oxide Leaching Process from Aku Clay**

Run order	Calcination temperature ( $^{\circ}\text{C}$ )		Leaching temperature ( $^{\circ}\text{C}$ )		Acid concentration ( $\text{mol}/\text{dm}^3$ )		Liquid-solid ratio ( $\text{cm}^3/\text{g}$ )		Contact time (min)	
	A		B		C		D		E	
	Coded	Real	Coded	Real	Coded	Real	Coded	Real	Coded	Real
1	-1	700	-1	50	-1	1.5	-1	8	+1	80
2	+1	900	-1	50	-1	1.5	-1	8	-1	40
3	-1	700	+1	90	-1	1.5	-1	8	-1	40
4	+1	900	+1	90	-1	1.5	-1	8	+1	80
5	-1	700	-1	50	+1	3	-1	8	-1	40
6	+1	900	-1	50	+1	3	-1	8	+1	80
7	-1	700	+1	90	+1	3	-1	8	+1	80
8	+1	900	+1	90	+1	3	-1	8	-1	40
9	-1	700	-1	50	-1	1.5	+1	16	-1	40
10	+1	900	-1	50	-1	1.5	+1	16	+1	80
11	-1	700	+1	90	-1	1.5	+1	16	+1	80
12	+1	900	+1	90	-1	1.5	+1	16	-1	40
13	-1	700	-1	50	+1	3	+1	16	+1	80
14	+1	900	-1	50	+1	3	+1	16	-1	40
15	-1	700	+1	90	+1	3	+1	16	-1	40
16	+1	900	+1	90	+1	3	+1	16	+1	80
17	-2	600	0	70	0	2.25	0	12	0	60
18	+2	1000	0	70	0	2.25	0	12	0	60
19	0	800	-2	30	0	2.25	0	12	0	60
20	0	800	+2	110	0	2.25	0	12	0	60
21	0	800	0	70	-2	0.75	0	12	0	60
22	0	800	0	70	+2	3.75	0	12	0	60
23	0	800	0	70	0	2.25	-2	4	0	60
24	0	800	0	70	0	2.25	+2	20	0	60
25	0	800	0	70	0	2.25	0	12	-2	20
26	0	800	0	70	0	2.25	0	12	+2	100
27	0	800	0	70	0	2.25	0	12	0	60
28	0	800	0	70	0	2.25	0	12	0	60
29	0	800	0	70	0	2.25	0	12	0	60
30	0	800	0	70	0	2.25	0	12	0	60
31	0	800	0	70	0	2.25	0	12	0	60
32	0	800	0	70	0	2.25	0	12	0	60

### III RESULTS AND DISCUSSION

#### 3.1 Physico-chemical characterization and properties of the raw and calcined clays

Physico-chemical properties of the raw and calcined clay are presented in Table 3.1. From the table, it was observed that most of the properties increased after calcination except carbon and organic matter. The porosity was observed to have increased after calcination owing to increase in bulk density (Gray et al., 2014) enabling the leaching solvent to easily permeate the clay and enhance leaching.

**Table 3.1: Physico-chemical characterization of the clay samples**

Sample	pH	Surface Area ( $\text{cm}^2/\text{g}$ )	Bulk Density ( $\text{g}/\text{cm}^3$ )	Carbon (%)	Organic Matter (%)	Loss on Ignition (%)	Particle Density ( $\text{g}/\text{cm}^3$ )	Colour	Total Porosity (%)
Raw Clay	5.66	768.30	1.79	2.03	6.01	9.50	2.33	Light Brown 8/1	23.60
Calcined Clay	7.50	847.15	1.91	1.22	3.63	11.50	3.55	Brownish Gray 4/1	46.25

### 3.2 Atomic Absorption Spectrophotometer (AAS) characterization of the clay samples

AAS results are presented as shown in Table 3.2. It shows the concentration of different elements that are present in the clay samples. From the result, it is observed that the major elements in Aku clay are alumina, iron and sodium while traces of elements such as potassium, manganese, calcium, nickel were also observed. The biggest element in terms of composition in Aku clay was aluminum and iron.

**Table 3.2: AAS characterization of Aku clay**

Elemental symbol	Aku Clay Concentration (ppm)
Al	31.4739
Fe	26.6340
Na	9.5033
K	0.2833
Mn	0.3203
Ca	0.1314
Ni	0.2067
Mg	0.0325
Cu	0.0264
Zn	0.0180

### 3.3 Scanning Electron Microscopy (SEM) characterization of virgin and leached clay samples

SEM micrographs of the virgin and leached clay sample are provided in figs 3.1 and 3.2. Fig 3.1 represents the SEM image of the virgin clay 30 $\mu$ m. It was observed from the figure that the clay is a bulk of microstructure which in turn is composed of a homogeneously distributed network comprised of small filamentous and fistulous crystallites showing the presence of minerals. In the matrix, Luminous and non-luminous features can be seen. These features indicate the presence of minerals distributed in the organic matrix and as surface coverage. Some features such as fissures, cleats, cracks and veins can also be seen. The bright luminosity indicates the presence of lithophytes like magnesium, aluminum, silicon, calcium, titanium etc, and sidrophile, like iron. etched pits, layers, some islands and hills and valleys can be seen randomly distributed throughout the micrograph. These might be resulted from the calculations of dolomite like  $\text{CaMg}(\text{CO}_3)_2$  and calcites like  $\text{CaCO}_3$ , or their assemblage due to the thermal shock during metamorphism. Some discrete and coherent crystals (framboids, and entedral) of irregular shapes represent the presence of iron. Veins corresponding to iron oxides can also be seen. It is inferred that Aku clay under study contains large proportions of silica, calcium carbonate as well as some proportions of elements such as aluminum, iron, and potassium.

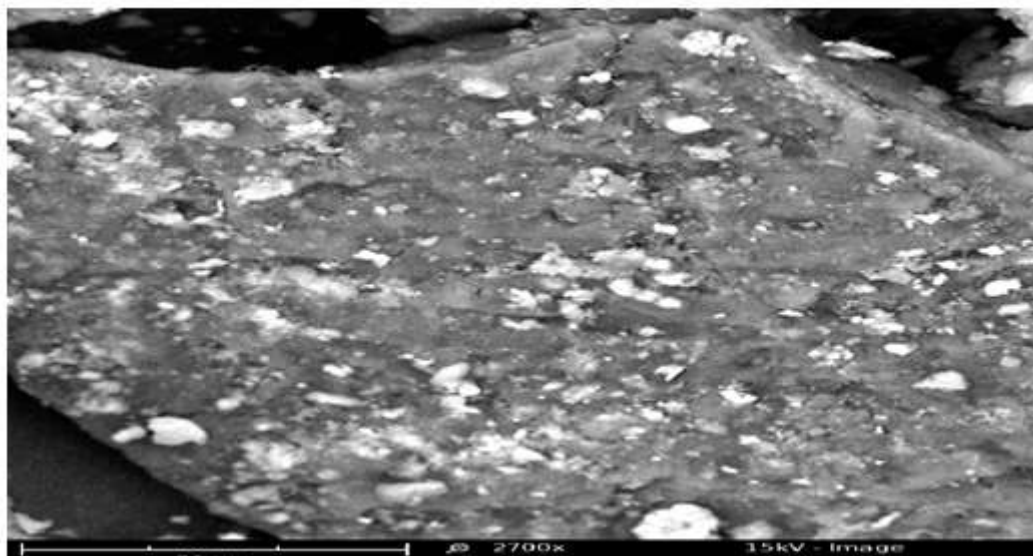


**Fig 3.1: SEM image of Aku Virgin clay sample @30 $\mu$ m**

It was observed from fig. 3.2 that the porosity increased and provides strong evidence that significant amount of inorganic elements were removed. However the surface coverage is still bright and luminous indicating the presence of mineral phases. It was observed that in the micrograph, the leachant (Conc. HCl) did enormous harm to the surface when compared to the virgin clay. Some minute fissures and cracks, however an evident. The surface was bright and mostly protracted. Some islands can also be seen. However the leachant

(HCL) used with the combination of factors for this experiment seem to be effective in leaching of the clay under study.

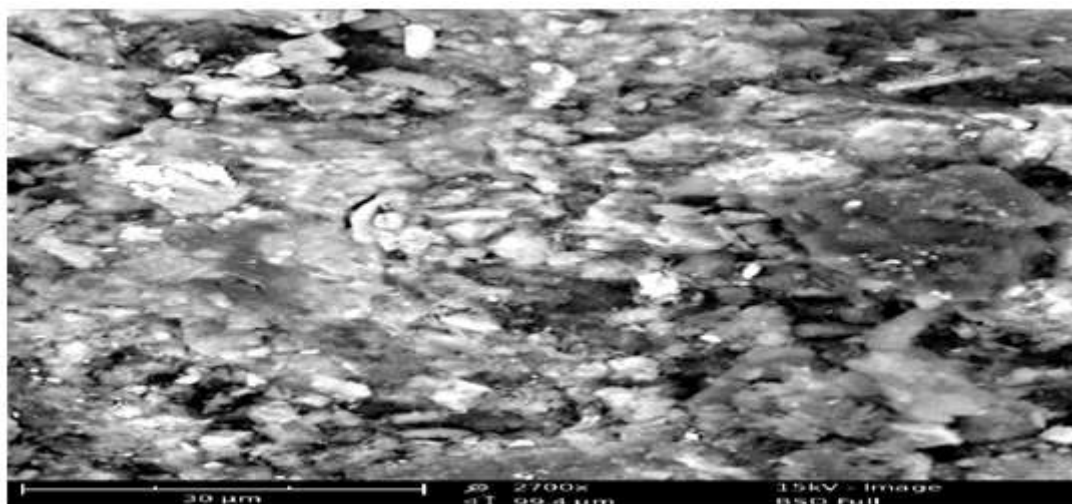


Fig 3.2: SEM image of Leached Clay @ 30µm

### 3.4 Fourier Transform Infrared (FTIR) characterization of raw, activated and leached clay

Fourier Transform Infrared (FTIR) studies of the raw, calcined and leached clay samples were carried out to determine the functional groups present in the clay samples. The coupled vibrations are appreciable due to the availability of various constituents. The IR spectra of raw, calcined and leached clays are shown in Table 3.3. The observed bands (in the range, 4000–400  $\text{cm}^{-1}$ ) have been tentatively assigned. In the IR studies of the samples, the Si–O stretching vibrations were observed at 779.48  $\text{cm}^{-1}$ , 644.38  $\text{cm}^{-1}$ , 582.62  $\text{cm}^{-1}$ , 505.42  $\text{cm}^{-1}$  and 428.22  $\text{cm}^{-1}$  in clay showing the presence of quartz (Udeigwe *et al.*, 2015). The appearance of  $\nu$  (Si–O–Si) and  $\delta$  (Si–O) bands also support the presence of quartz (Udeigwe *et al.*, 2015), a strong band from 3397.7  $\text{cm}^{-1}$  to 3404.64  $\text{cm}^{-1}$  indicate the possibility of the hydroxyl linkage. However, a broad band at 3446.74  $\text{cm}^{-1}$ , 3404.28  $\text{cm}^{-1}$  and a band at 1775.36  $\text{cm}^{-1}$ , 1624.82  $\text{cm}^{-1}$  in the spectra of raw and calcined clays suggest the possibility of water of hydration in the clay.

The inter layer hydrogen bonding in clay is assigned by a characteristics band at 3662.9  $\text{cm}^{-1}$ . Most of the bands such as 3740.1  $\text{cm}^{-1}$ , 3662.9  $\text{cm}^{-1}$ , 3404.28  $\text{cm}^{-1}$ , 1049.68  $\text{cm}^{-1}$ , 918.44  $\text{cm}^{-1}$ , 779.4  $\text{cm}^{-1}$ , 644.38  $\text{cm}^{-1}$ , 582.62  $\text{cm}^{-1}$ , 505.42  $\text{cm}^{-1}$ , and 428.22  $\text{cm}^{-1}$  show the presence of kaolinite. The vibrations observed at 984.06  $\text{cm}^{-1}$  and 918.44  $\text{cm}^{-1}$  indicate the possibility of the presence of hematite. The presence of bands at 3740.1  $\text{cm}^{-1}$ , 3662.9  $\text{cm}^{-1}$ , 3404.28  $\text{cm}^{-1}$ , 2998.98  $\text{cm}^{-1}$  to 2091.30  $\text{cm}^{-1}$ , 1775.36  $\text{cm}^{-1}$ , 1624.82  $\text{cm}^{-1}$ , 1103.72  $\text{cm}^{-1}$ , 1049.69  $\text{cm}^{-1}$ , 918.44  $\text{cm}^{-1}$  and 779.48  $\text{cm}^{-1}$  indicate the possibility of the presence of illite, whereas 3662.9  $\text{cm}^{-1}$ , 1624.82  $\text{cm}^{-1}$ , 1775.36  $\text{cm}^{-1}$ , 1049.69  $\text{cm}^{-1}$  are indicative of gypsum and 644.38  $\text{cm}^{-1}$  shows the possibility of the presence of calcite. Thus the results of IR are quite helpful in the identification of various forms of minerals present in the clay. IR spectra of these raw and calcined clay show band at 3662.9  $\text{cm}^{-1}$  corresponding to  $\text{H}_2\text{O}$  vibrations, indicating the hydrous nature of these materials and the presence of hydroxyl linkage. However, owing to the mixing of various overtones and complexity of the spectrum of clay, distinct assignments of various other vibrations have not been made. Some bands were absent in the calcined clay compare to those of raw clay (Table 5) and this could be that calcination removed some volatile materials present in the clay thereby making leaching of minerals easier. The bands of leached clay appeared to be similar to bands of raw clay showing that leaching was carried out in the calcined clay (Table 3.3). It also has the same range of wavelength with similar functional group as the raw clay and calcined clay.

Table 3.3: FTIR characterization of raw, calcined and leached clay samples

Raw clay	Assignment	Calcined clay	Leached clay
Frequency ( $\text{cm}^{-1}$ )	Assignment	Frequency ( $\text{cm}^{-1}$ )	Frequency ( $\text{cm}^{-1}$ )
3630.4 – 3971.7	O-H stretch	3662.9-3940.82	3608.9-3956.26
3504.64-3581.84	Hydroxyl group, H-bonded, O-H stretch	3570.26	3527.8
3327.08	NH stretch	3357.96-3446.74	3300.06-3384.98
3172.68-3234.44	Aliphatic secondary amine, NH stretch	3203.56	3045.06-3230.58
2852.3-3060.74	Normal “polymeric” OH stretch	2998.98-3080.04	2890-2952.66

2612.98-2736.5	Methylamino, N-CH <sub>3</sub> , C-H stretch	2713.34-2805.98	2609.12-2890.9
2211.54-2489.46	Isocyanate (-N=C=O asym. Stretch)	2091.88-2585.96	2304.18-2516.48
2138.20	Cynaide ion, thiocyanate ion and related ions	2083.6	2099.6-2215.4
1906.6-1964.5	Aromatic combination	19837.48	1902.74-1999.24
1775.36	Conjugated ketone, open-chain acid anhydride	1624.82-1871.82	16886.58-1833.26
1570.78	C=C-C Aromatic ring stretch	-	1593.94
1443.4	O-H bend	-	1447.26
1219.52-1381.64	N-O asymmetric stretch	1397.08	1350.76
1184.78	Aromatic C-H in plane bend	-	1177.06
1049.68	Organic siloxane, Si-O-Si	1103.72	1011-.08-1107.58
918.44	Silicate ion	918.44-984.06	918.44
-	Peroxides, C-O-O- stretch	856.68	825.80
779.48	C-Cl stretch, Alkyne C-H bend	767.9	737.02
428.22-644.38	C-Cl stretch, Alkyne C-H bend, Si-O stretching	435.94-644.38	424.36-640.52

### 3.5 Optimization of leaching of iron oxide from 'Aku' clay

To optimize the leaching of iron oxide, Central Composite Design (CCD) of Response Surface Methodology (RSM) was used to analyze significance of the model and determination of the optimum values of the leaching variables. The actual yield of iron oxide from each experimental run are presented as shown in table 3.4.s

**Table 3.4: Yield of iron oxide using design matrix**

Run	A:Calcination temperature Deg. Cel.	B:Leaching temperature Deg. Cel.	C:Acid concentration mol/dm <sup>3</sup>	D:Liquid-solid ratio ml/g	E:Contact time Minutes	Yield of iron oxide %
1	700	50	1.5	8	80	41.5
2	900	50	1.5	8	40	52
3	700	90	1.5	8	40	43
4	900	90	1.5	8	80	49
5	700	50	3	8	40	47
6	900	50	3	8	80	52
7	700	90	3	8	80	42
8	900	90	3	8	40	46.2
9	700	50	1.5	16	40	57
10	900	50	1.5	16	80	56
11	700	90	1.5	16	80	51
12	900	90	1.5	16	40	47
13	700	50	3	16	80	44.8
14	900	50	3	16	40	54.9
15	700	90	3	16	40	35.9
16	900	90	3	16	80	59
17	600	70	2.25	12	60	46
18	1000	70	2.25	12	60	57.9
19	800	30	2.25	12	60	57
20	800	110	2.25	12	60	50
21	800	70	0.75	12	60	59.7
22	800	70	3.75	12	60	56.6
23	800	70	2.25	4	60	49
24	800	70	2.25	20	60	57
25	800	70	2.25	12	20	46.6
26	800	70	2.25	12	100	53
27	800	70	2.25	12	60	69.2
28	800	70	2.25	12	60	68
29	800	70	2.25	12	60	69.2
30	800	70	2.25	12	60	68
31	800	70	2.25	12	60	69.2
32	800	70	2.25	12	60	68

### 3.6 Analysis of variance (ANOVA) for leaching of iron oxide

The Analysis of variance of the result of the experiments in table 3.4 was carried out. The percentage yield of iron oxide extracted depends on the results if the interaction between the process parameters is significant. Using the same Design expert version 9.0.7.1, Equation 2 was obtained as the quadratic equation that fitted the data.

$$Y_{\text{iron oxide}} = 68.75 + 3.24A - 1.92B - 0.87C + 2.04D + 1.05E + 0.29AB + 1.93AC + 0.16AD + 1.22AE + 0.056BC - 0.47BD + 2.84BE - 1.13CD + 0.96CE + 1.23DE - 4.31A^2 - 3.92B^2 - 2.76C^2 - 4.05D^2 - 4.85E^2 \quad (2)$$

Table 3.5: Analysis of variance table for the yield of iron oxide

Source	Coefficient estimate	Degree of freedom	Sum of square	Mean Square	F-value	P-value (Prob >F)
Model	68.75	20	2576.63	128.83	141.91	< 0.0001
A	3.24	1	251.55	251.55	277.10	< 0.0001
B	-1.92	1	88.55	88.55	97.54	< 0.0001
C	-0.87	1	18.20	18.20	20.05	0.0009
D	2.04	1	99.63	99.63	109.75	< 0.0001
E	1.05	1	26.25	26.25	28.92	0.0002
AC	1.93	1	59.68	59.68	65.74	< 0.0001
AE	1.22	1	23.77	23.77	26.18	0.0003
BE	2.84	1	129.39	129.39	142.53	< 0.0001
CD	-1.13	1	20.48	20.48	22.55	0.0006
CE	0.96	1	14.63	14.63	16.12	0.0020
DE	1.23	1	24.26	24.26	26.72	0.0003
A <sup>2</sup>	-4.31	1	544.67	544.67	599.98	< 0.0001
B <sup>2</sup>	-3.92	1	451.11	451.11	496.93	< 0.0001
C <sup>2</sup>	-2.76	1	223.30	223.30	245.98	< 0.0001
D <sup>2</sup>	-4.05	1	480.33	480.33	529.11	< 0.0001
E <sup>2</sup>	-4.85	1	689.02	689.02	759.00	< 0.0001
Residual			9.99	0.91		
Cor. Total			2586.61			

Std. Dev. = 0.95; Mean = 53.83; C.V.% = 1.77; PRESS = 201.72; R<sup>2</sup> = 0.9961; Adj. R<sup>2</sup> = 0.9891; Pred. R<sup>2</sup> = 0.9220; Adeq. Precision = 42.311

The Analysis of variance (ANOVA) results for the model terms are given in Table 3.5. The result was also applied for estimating the significance of the model at 5% significance level as shown in Table 3.5. A model is considered significant if the p-value (significance probability value) is less than 0.05. From the p-values presented in Table 3.5, it can be deduced that all the linear terms A, B, C, D and E and interaction terms AC, AE, BE, CD, CE, DE and quadratic terms A<sup>2</sup>, B<sup>2</sup>, C<sup>2</sup>, D<sup>2</sup>, and E<sup>2</sup> were significant model terms. Based on this, the insignificant terms (AB, BD and AD) of the model were removed and the model reduced to the following equation

$$Y_{\text{iron oxide}} = 68.75 + 3.24A - 1.92B - 0.87C + 2.04D + 1.05E + 1.93AC + 1.22AE + 2.84BE - 1.13CD + 0.96CE + 1.23DE - 4.31A^2 - 3.92B^2 - 2.76C^2 - 4.05D^2 - 4.85E^2 \quad (3)$$

The experimental data in Table 3.4 were also analyzed to check the correlation between the experimental and predicted iron oxide yield. The normal probability versus residual plot, and actual versus predicted plot are shown in Figs. 3.3 and 3.4 respectively. It can be seen from the Figures that the data points on the plot were reasonably distributed near to the straight line, indicating a good relationship between the experimental and predicted values of the response, and that the underlying assumptions of the above analysis were appropriate. The result also suggests that the selected quadratic model was adequate in predicting the response variables for the experimental data.

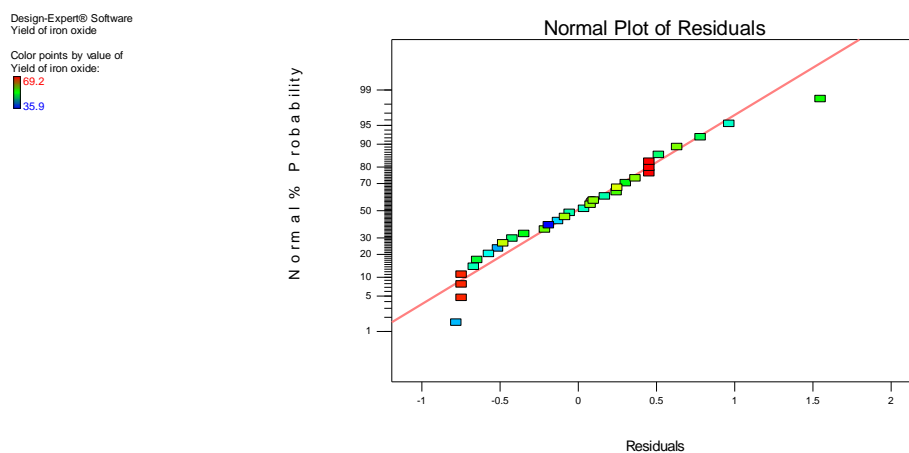


Fig 3.3: Plot of normal probability versus residuals iron oxide yield.

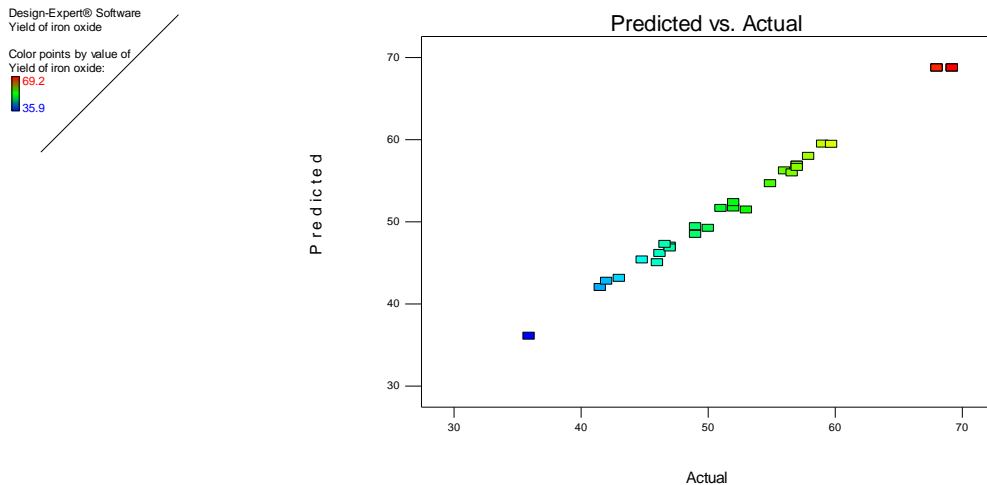


Fig 3.4: Plot of predicted versus actual iron oxide yield.

### 3.7 Surface Plots for iron oxide yield

The 3D response surface plots were generated to estimate the effect of the combinations of the independent variables on the iron oxide yield. The plots are shown in Figs. 3.5 to 3.10. Fig. 3.5 showed the dependency of iron oxide yield on the interaction of calcination temperature and acid concentration. As can be seen from figure 3.5, percentage iron oxide yield increases as both the calcination temperature and acid concentration increases up to the mid point of these variables and then decreased beyond 2.4M of acid concentration and 850°C calcination temperature. This could be due to total dehydration and solid-phase transformation of Iron oxide at mid point of the variables. It could also be due to sintering effect at higher calcination temperature.

Fig. 3.6 shows the dependency of iron oxide yield on calcination temperature and contact time. As can be seen from the figure, percentage iron oxide yield increases as both the calcination temperature and contact time increases up to the mid point of these variables and then decreased beyond 70 minutes contact time and 850°C calcination temperature. This could be due to sintering effect of high calcinations temperature.

Fig. 3.7 shows the dependency of iron oxide yield on leaching temperature and contact time. As can be observed from the figure, percentage iron oxide yield increases as both the leaching temperature and contact time increases up to the mid point of these variables and then decrease. This may be that beyond the midpoints of these variables, the conditions were no longer favorable for leaching as a result of high temperature.

Fig. 3.8 shows the dependency of iron oxide yield on acid concentration and liquid to solid ratio. As can be seen from the figure, percentage iron oxide yield increases as both the acid concentration and liquid to solid ratio increases up to the mid point of these variables and then decrease. This could be attributed to unfavourable conditions (high acid concentration) for leaching beyond the midpoints of these variables.

Fig. 3.9 shows the dependency of iron oxide yield on acid concentration and contact time. As can be observed from the figure, percentage iron oxide yield increases as both the acid concentration and contact time increases up to the mid point of these variables and then decreased. This may be that beyond the midpoints of these variables, the conditions were no longer favourable for leaching.

Fig. 3.10 shows the dependency of iron oxide yield on contact time and liquid to solid ratio. As can be seen from the figure, percentage iron oxide yield increases as both the contact time and liquid to solid ratio increased up to the mid point of these variables and then decreased. This could be that beyond the midpoints of these variables, the conditions were no longer favourable for leaching.

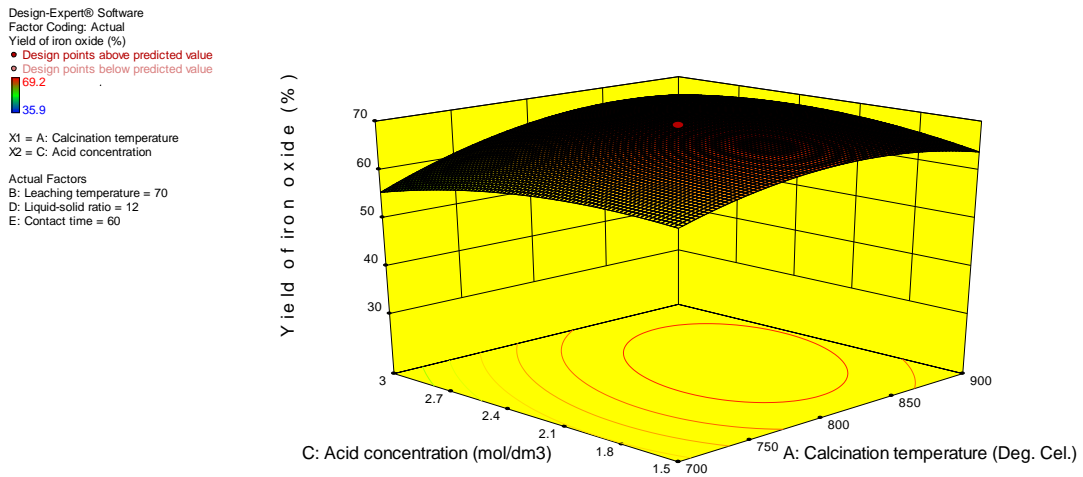


Fig. 3.5: 3D plots showing the effect of calcination temperature and acid concentration on the iron oxide yield

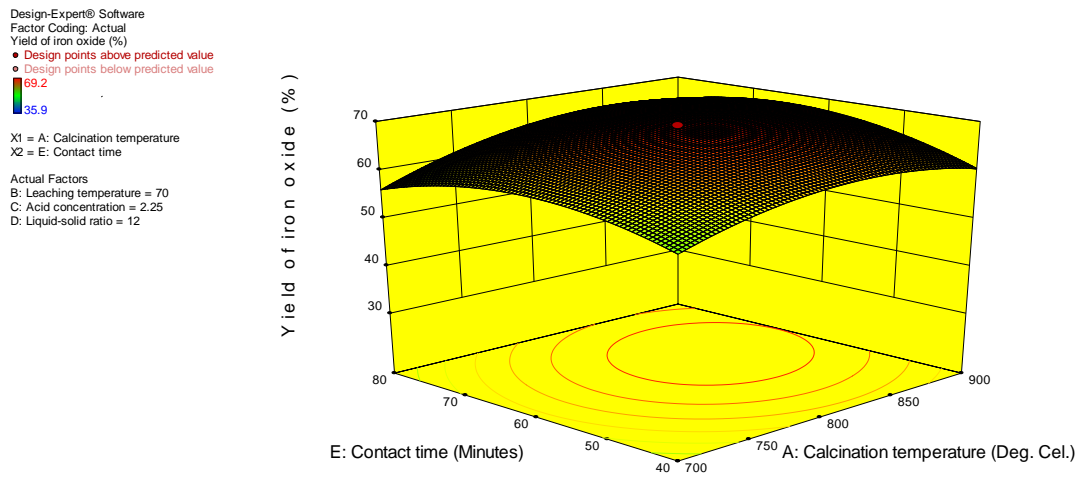


Fig. 3.6: 3D plots showing the effect of calcination temperature and contact time on the iron oxide yield

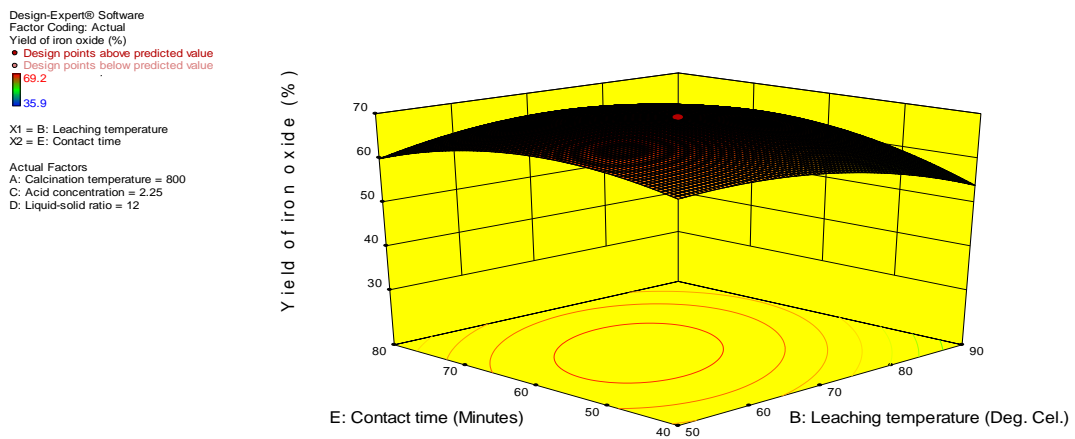


Fig. 3.7: 3D plots showing the effect of leaching temperature and contact time on the iron oxide yield

Design-Expert® Software  
 Factor Coding: Actual  
 Yield of iron oxide (%)  
 ● Design points above predicted value  
 ● Design points below predicted value  
 69.2  
 35.9  
 X1 = C: Acid concentration  
 X2 = D: Liquid-solid ratio  
 Actual Factors  
 A: Calcination temperature = 800  
 B: Leaching temperature = 70  
 E: Contact time = 60

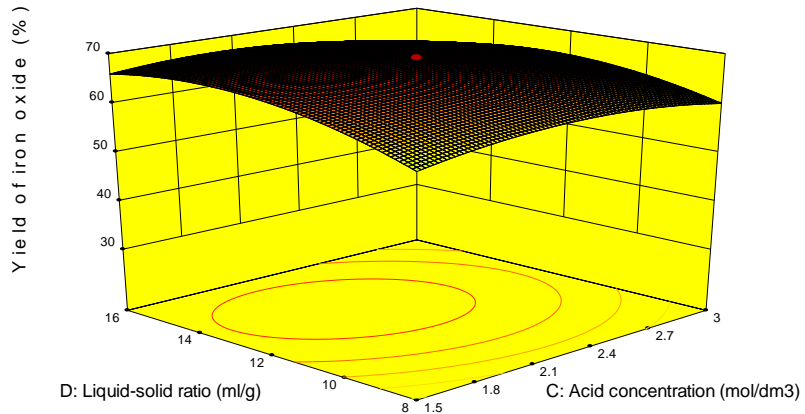


Fig. 3.8: 3D plots showing the effect of acid concentration and liquid to solid ratio on the iron oxide yield

Design-Expert® Software  
 Factor Coding: Actual  
 Yield of iron oxide (%)  
 ● Design points above predicted value  
 ● Design points below predicted value  
 69.2  
 35.9  
 X1 = C: Acid concentration  
 X2 = E: Contact time  
 Actual Factors  
 A: Calcination temperature = 800  
 B: Leaching temperature = 70  
 D: Liquid-solid ratio = 12

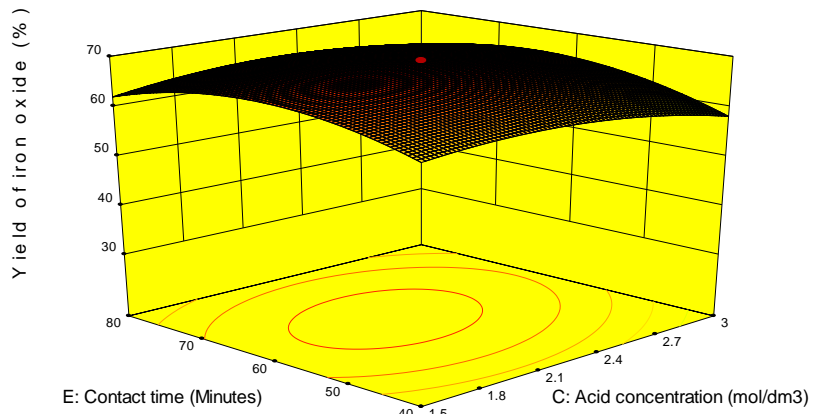


Fig. 3.9: 3D plots showing the effect of acid concentration and contact time on the iron oxide yield

Design-Expert® Software  
 Factor Coding: Actual  
 Yield of iron oxide (%)  
 ● Design points above predicted value  
 ● Design points below predicted value  
 69.2  
 35.9  
 X1 = D: Liquid-solid ratio  
 X2 = E: Contact time  
 Actual Factors  
 A: Calcination temperature = 800  
 B: Leaching temperature = 70  
 C: Acid concentration = 2.25

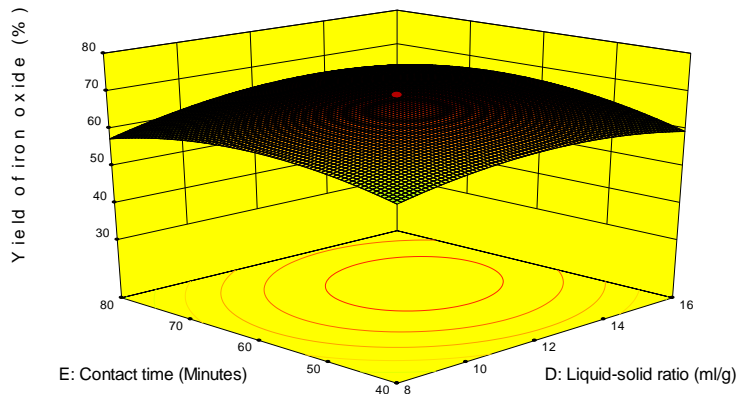


Fig 3.10: 3D plots showing the effect of contact time and liquid to solid ratio on the iron oxide yield

**Table 3.6: Predicted and Experimental values for iron oxide yield**

Calcination Temperature (°C)	Leaching Temperature (°C)	Acid Concentration (mol/dm <sup>3</sup> )	Liquid to solid Ratio (ml/g)	Contact Time (minutes)	Experimental Yield (%)	Predicted Yield (%)
822	67	2.2	12.9	61	68.9	69.78

The leaching of iron oxide under the obtained optimum operating conditions was carried out in order to evaluate the precision of the quadratic model; the experimental value and predicted values as shown in Table 3.6. Comparing the experimental and predicted Iron oxide yields, it was observed that the error between the experimental and predicted was 1.2%, therefore it can be concluded that the generated model had sufficient accuracy to predict the iron oxide yield.

### 3.8 PERCENTAGE OF METALLIC OXIDES IN THE EXTRACT

The leached extract/sample was characterized with X-Ray fluorescence spectrometer and the result presented in Table 3.7. From the table, it could be observed that percentage iron oxide in the metallic oxide is 54.103 wt%. This shows that iron oxide was extracted but requires further purification.

**Table 3.7: Percentage composition of the leached extract**

Compound	Concentration (wt %)
Na <sub>2</sub> O	0.441
MgO	1.061
Al <sub>2</sub> O <sub>3</sub>	16.404
SiO <sub>2</sub>	8.923
P <sub>2</sub> O <sub>5</sub>	1.176
SO <sub>3</sub>	0.910
Cl	14.818
K <sub>2</sub> O	0.028
CaO	1.745
TiO <sub>2</sub>	0.206
Cr <sub>2</sub> O <sub>3</sub>	0.017
Mn <sub>2</sub> O <sub>3</sub>	0.137
<b>Fe<sub>2</sub>O<sub>3</sub></b>	<b>54.103</b>
ZnO	0.017
SrO	0.042

### REFERENCES

- [1]. ASTM D7263-09. Standard Test Methods for Laboratory Determination of Density (Unit Weight) of Soil Specimens, ASTM International, West Conshohocken, PA, 2017, www.astm.org accessed October, 2017.
- [2]. Housecroft, C. E., Sharpe, A. G. "Chapter 22: d-block metal chemistry: the first row elements". Inorganic Chemistry, 3rd Edition. Pearson. (2008) p.716.
- [3]. Coulson, J., Richardson, F., Backhurst, J., Harker, J. Chemical Engineering, Vol. 2, 4<sup>th</sup> Edition. Pergamon Press, Oxford, Uk., 234-236; (1991) 412,417.
- [4]. Gray, M., Johnson, M. G., Dragila, M. I., & Kleber, M. Water uptake in biochars: The roles of porosity and hydrophobicity. Biomass and Bioenergy, 61, (2014) 196-205. doi:10.1016/j.biombioe.2013.12.010
- [5]. Udeigwe U., Onukwuli, O. D., Ajemba R., Ude C. N. Kinetics studies of hydrochloric acid leaching of alumina from Agbaja clay. International Journal of Research in Advanced Engineering and Technology, 1(1), (2015) 64-72.
- [6]. Arturo, I., Martinez, M.A., Garcia-Lobato, Dale L. P. Study of the Properties of Iron Oxide Nanostructures. In: Research in Nanotechnology Developments, (2009) pp 183-194. Nova Science Publishers, Inc., Ramos Arizpe, Coahuila, Mexico.
- [7]. Sultana, U. K., Gulshan, F., Kumy, A. S. W. Kinetics of leaching of iron oxide in clay in oxalic acid and in hydrochloric acid solutions. *Materials Science and Metallurgy Engineering*, 2(1), (2014) 5-10.
- [8]. Alafara, A., Adekola, F., Folashade, A. Quantitative leaching of iron ore in hydrochloric acid. *Journal of Applied Science*, 9(3). (2005) 15-20.
- [9]. Ajemba, R., Onukwuli O. Process Optimization of Sulphuric acid Leaching of Alumina from Nteje Clay using Central Composite Rotatable Design: International Journal of Multidisciplinary sciences and Engineering, 3(5), (2012) 116-121.
- [10]. Ajemba, R.O., Onukwuli, O.D. Kinetic Model for Ukpok Clay Dissolution in Hydrochloric acid solution: Journal of Emerging Trends in Engineering and Applied Sciences. 3 (3): (2012) 448-454.
- [11]. Ambikadevi, V., Lalithambika, M. Effects of Organic Acids on Ferric Iron Remonal from Iron-stained Kaolinite. Appl clay Sci.16, 133-145. and its application to Injection Molding Processes with Numerical Analysis. Journal of Materials Processing Technology, 146, (2000) 221 – 227.
- [12]. Ogbemudia, J., Felix, O. and Uzoma N. Characterization of Ugbegun clay deposit for its potential, International Journal of chemistry research, 1(2) (2010).
- [13]. Ogbuagu, J., Asuzu, A., Igbokwe, P. Characterization and utilization of kaolin mineral deposits in Ukpok Anambra State Nigeria. *NJERD*, (2007) 6(2).
- [14]. Poppleton, H., Sawyer, D. Hydrochloric Acid Leaching of Calcined Kaolin to Produce Alumina-Instruments and Experimental Techniques. English Translation of Pribory I Tekhnika Eksperimenta, 2, (1977) 103-114.
- [15]. Orugba, O.H., Onukwuli, O.D., Njoku, N.C. Process modeling of sulphuric acid leaching of Iron from Ozoro clay. European Scientific Journal, Vol. 10; (2014) No. 30 ISSN: 1857-7881.

- [16]. Rasmita, B., Mamatam M. Facile precipitation and phase formation of Iron Oxide with in situ Fe(II) in  $\text{Fe}_2(\text{SO}_4)_3\text{-NaOH-(N}_2\text{H}_4)_2\text{H}_2\text{SO}_4\text{-H}_2\text{O}$  medium. *Indian Journal of Chemical Technology*. 18, (2011) 107-112.
- [17]. Suong, O., L., Tam T., Yi Y., P., Seong J., K., MyongJun, K. Study on the kinetics of Iron oxide leaching by oxalic acid, *Int. J. Miner. Process.* 80, (2006) 144-152.
- [18]. Eisele, J., Bauer, J., Shanks, D. Bench-Scale Studies to Recover Alumina from Clay by a Hydrochloric Acid Process. *Industrial & Engineering Chemistry, Product Research and Development*, 22(1), 105-110. *European Scientific Journal* October 2014 edition vol.10, No.30 (1983) ISSN: 1857-7881 (Print) e-ISSN 1857-7431.
- [19]. Al-Zahrani, A. A., Abdul-Majid, M. H. Extraction of alumina from local clays by hydrochloric acid process. *Journal of King Abdulaziz University : Engineering Sciences*, 20(2): (2009) 29-41.
- [20]. Ozdemir, M., Cetisli, H. Extraction kinetics of alumina in sulphuric acid and hydrochloric acid. *Hydrometallurgy*, 76(3-4): (2005) 217-224.

Onoh Ikechukwu Maxwell." Optimization and Process Modelling Of the Extraction of Iron Oxide from Aku Clay by Hydrochloric Acid Leaching."American Journal Of Engineering Research (AJER), Vol. 7, No. 6, 2018, Pp.87-98.